October 2018

Laser-induced Ultrafast Transport and Demagnetization at the Earliest Time: First-principles and Real-time Investigation

Thomas George
University of Missouri-St. Louis, tfgeorge@umsl.edu

G.P. Zhang
Indiana State University

Y. Bai
Indiana State University

T. Jenkins
Indiana State University

Journal of Physics: Condensed Matter

PAPER

Laser-induced ultrafast transport and demagnetization at the earliest time: first-principles and real-time investigation

To cite this article: G P Zhang *et al* 2018 *J. Phys.: Condens. Matter* **30** 465801

IOP Publishing Journal of Physics: Condensed Matter
J. Phys.: Condens. Matter **30** (2018) 465801 (11pp) https://doi.org/10.1088/1361-648X/aae5a9

Laser-induced ultrafast transport and demagnetization at the earliest time: first-principles and real-time investigation

G P Zhang[1], Y H Bai[2], Tyler Jenkins[1] and Thomas F George[3]

[1] Department of Physics, Indiana State University, Terre Haute, IN 47809, United States of America
[2] Office of Information Technology, Indiana State University, Terre Haute, IN 47809, United States of America
[3] Office of the Chancellor, Departments of Chemistry & Biochemistry and Physics & Astronomy, University of Missouri-St. Louis, St. Louis, MO 63121, United States of America

E-mail: gpzhang.physics@gmail.com

Received 3 August 2018, revised 20 September 2018
Accepted for publication 2 October 2018
Published 25 October 2018

Abstract

It is generally believed that there are at least two ways to use an ultrafast laser pulse to demagnetize a magnetic sample. One is to directly photo-demagnetize the system through spin–orbit coupling (SOC), and the other is to utilize ultrafast hot electron transport without SOC. The challenge is that these two processes are entangled on the same time scale. While the experimental results have been inconclusive, theoretical investigations are even scarcer, beyond those earlier studies based on spin superdiffusion. For instance, we do not even know how fast electrons move under laser excitation and how far they move. Here we carry out a first-principles time-dependent calculation to investigate how fast electrons actually move under laser excitation and how large the electron transport affects demagnetization on the shortest time scale. To take into account the transport effect, we implement the intraband transition in our theory. In the bulk fcc Ni, we find the effect of the spin transport on the demagnetization is extremely small, no more than 1%. The collective electron velocity in Ni is 0.4 Å fs^{-1}, much smaller than the Fermi velocity, and the collective displacement is no more than 0.1 Å. But this does not mean that electrons do not travel fast; instead we find that electron velocities at two opposite crystal momenta cancel each other. We follow the Γ-X line and find a huge dispersion in the velocities in the crystal momentum space. In the Fe/W(1 1 0) thin film, the overall demagnetization is larger than Ni, and the Fermi velocity is higher than Ni. However, the effect of the spin transport is still small in the Fe/W(1 1 0) thin film. Based on our numerical results and existing experimental findings, we propose a different mechanism that can explain two latest experimental results. Our finding sheds new light on the effect of ballistic transport on demagnetization.

Keywords: ultrafast demagnetization, transport, laser-induced, crystal momentum, intraband transitions, interband transitions

(Some figures may appear in colour only in the online journal)

1. Introduction

Interaction between light and magnetism has a long history and can be traced back to Faraday, Kerr and Voigt effects. Using light to control and manipulate magnetic properties has become a focus of research. Over two decades ago, Beaurepaire and coworkers [1] discovered that a 60 fs laser pulse could demagnetize a ferromagnetic nickel thin film within 1 ps. The film was 22 nm thick, coated with a 100 nm MgF_2. However, its underlying mechanism is under intense debate [2–5]. We proposed a model (Hübner model) [2, 6] that is based on the direct interaction of the laser field and

spin system via spin–orbit coupling. The spin–orbit coupling is necessary since it breaks the spin symmetry and allows the electron to transfer its spin to its orbital degree of freedom and back [7]. This is different from the magnon picture, where the demagnetization is perceived as the number of magnon increases as temperature increases, and because the total spin is still a good quantum number, one has to manually break the spin symmetry when temperature changes. In the Hübner model, electrons are itinerant and mobile. The demagnetization is realized because the spin expectation value is smaller in conduction bands than valence bands close to the Fermi surface. Koopmans *et al* [3] proposed a similar model by emphasizing on spin mixing and spin flipping through the phonon interaction. Naturally, spin mixing and spin flipping are also included in the Hübner model. The key difference between the Koopmans model and Hübner model is the way that the spins move out of the system.

Battiao *et al* proposed a different model, the spin superdiffusion model (SSD) [8, 9]. SSD does not need the spin–orbit coupling, but relies on the difference between majority spin and minority spin diffusions. Since majority spins move faster than minority spins, this creates a depletion zone for majority spins. Assuming the minority spins stay, loss of the majority spins in the excited regions leads to demagnetization. They argued that SSD can even completely explain the ultrafast demagnetization [8]. Melnikov *et al* [10] carried out the second-harmonic generation measurement and found that upon laser pumping on the Fe layer, the gold layer becomes spin polarized with a clear hysteresis loop. However, this experiment only showed the spin transport out of Fe to Au layer, and did not prove that SSD is responsible for demagnetization. Vodungbo *et al* [11] examined a faster demagnetization (within 100 fs) in CoPd multilayers, with each stack as 1 nm thick. They found no modification of the magnetic structure and the resonant magnetic scattering patterns peaks at the same wave vector transfer. Nevertheless, they assigned this finding to the direct transfer of spin angular momentum between neighboring domains. About one month later, Pfau *et al* [12] carried out a similar experiment in CoPt multilayers and reached a different conclusion that the peak of the small-angle x-ray scattering shifts with time.

Two days later after Pfau's submission, Rudolf *et al* [13] reported that the ultrafast magnetization enhancement was driven by a superdiffusive spin current. They found that in the Ni/Ru/Fe trilayers if the magnetizations in the Ni and Fe layers are parallel to each other, the magnetization in the Fe layer increases. However, the amount of decrease in the Ni layer is not equal to the amount of increase in the Fe layer. In addition, they found that there is a laser fluence limit of 2.0 mJ cm^{-2}, beyond which only the demagnetization is observed. They argued that this was due to the spin superdiffusion saturation.

Eschenlohr *et al* [14] identified the ultrafast spin transport as the sole mechanism for femtosecond demagnetization, excluding spin-flips that are directly induced through the spin-laser field interaction [2, 15, 16]. They showed that SSD could accurately explain their observation. Experimentally, they employed x-ray circular dichroism to probe the spin change in an Au/Ni layered structure. They shined the light directly on to the thicker nonmagnetic Au layer, so the direct light excitation of Ni is smaller. In this case, only hot electrons hit the nickel layer. They concluded that the fact that the Ni layer is demagnetized shows the transport is the dominant factor, which excludes other mechanisms such as spin flip or spin-laser interaction. Thus, they believed that they provided decisive arguments for unraveling the origin of ultrafast demagnetization. In the same year, Turgut *et al* [17] showed that in contrast to the earlier findings [8, 9, 14], the spin superdiffusion is not the only process that leads to the demagnetization. They found that if they reversed the order of the multilayer by placing the iron layer first and then the nickel layer, there is no spin enhancement. This shows that the appearance of spin diffusion is system dependent, not intrinsic to the demagnetization.

A more direct test is from the work by Schellenkens *et al* [18]. They grew wedged Ni films on both insulating sapphire and conducting aluminum substrates, exactly the same as those used in the theory [8, 9]. But to their surprise, the temporal evolution of the magnetization, regardless of whether it is pumped on the front or on the back of the sample, is identical. They argued that if back pumped, the spin should accumulate in the front, and when the probe pulse detects it, the outgoing signal should be increased. They also purposely reduced the laser intensity so SSD can play a role, but no influence of transport was found. However, the same group [19] reached a different conclusion lately for the Ni/Au system, where they had substantial evidence that the demagnetization was dominantly driven by spin currents. Moisan *et al* [20] showed that regardless of their sample magnetic configuration, the demagnetization time remains the same, and they concluded that hot electron spin transfer between neighboring domains does not change the ultrafast magnetization. However, they suggested that the effect of spin transport on demagnetization may be related to the spin accumulation length. von Korff Schmising *et al* [21] attempted to image the demagnetization dynamics using a holographic mask. They found a rapid lateral increase of the demagnetized area, with the propagation front moving with a speed on the order of 0.2 nm fs^{-1}. However it is difficult to correlate the demagnetization with the lateral increase.

Shokeen *et al* [22] employed a 10 fs pulse to probe the magnetization dynamics in Ni and Co systems of various thickness from 10 to 40 nm, and found that ultrafast demagnetization is again system dependent, and both spin majority and minority channels contribute, not that the majority alone contributes as assumed in the spin superdiffusion theory [8, 9]. An increase in Co was observed but on a time scale of 20 fs, far shorter than appropriate for SSD. In Co/Cu(0 0 1), Chen *et al* [23] further showed that demagnetization does not occur through redistribution of spin among Co and Cu atoms, though their TDDFT calculation is still unable to reproduce the same amount of spin moment reduction as their experiment. Tengdin *et al* [24] showed that demagnetization and the collapse of the exchange splitting in Ni are mediated by low-energy magnon, not SSD. However, magnon excitation permutes with the total spin, so it is puzzling why demagnetization could occur. In contrast to prior experimental results [3], they found that the demagnetization time is fluence independent and is 176 fs. The origin of the above experimental

discrepancy is unknown. A quasi-phase transition at 20 fs is attributed to both SSD and spin–orbit coupling. But on such a short time scale, transport on the 1 nm scale should be ballistic, not diffusive, while the spin–orbit coupling λ is too weak (20 fs corresponds to 0.205 eV, and in nickel $\lambda = 0.07$ eV [2]). In CoPt multilayers, Zhang *et al* [25] showed that the demagnetization is always at 150 fs, independent of external magnetic field amplitudes. If the spin transport between different magnetic domains were important to demagnetization, one would expect that the domain structure must affect the demagnetization. Their results show this is not the case. They attributed the local dissipation of spin angular momentum as a dominant channel to demagnetization. The material specific nature of demagnetization also appears in NiPd magnetic alloys. This is an ideal model system for SSD where Ni and Pd atoms are next to each other, so the expected spin superdiffusion should be very strong. However, Gang *et al* [26] concluded that the optically triggered spin current between the subsystems of Ni_xPd_{1-x} alloys does not dominate the demagnetization, in contrast to SSD [8, 9]. On the other hand, Ferté *et al* [27] showed that the hot-electron pulse can demagnetize CoTb alloys as well.

So far, there has been no consensus experimentally. A theoretical investigation at the initial stage of laser-induced demagnetization and transport is imperative. This would potentially allow one to extract useful insights from SSD and develop a new picture. In this paper, we employ the first-principles time-dependent Liouville density functional theory [28], without resorting to the empirical procedure [8, 9]. We take into account both the interband transition and intraband transitions (transport effect) among band states. We find that the effect of direct laser-induced transport on the demagnetization is very weak. In fcc Ni, the electron oscillates with a maximum collective velocity amplitude of 0.4 Å fs^{-1}, far below the Fermi velocity, and a net displacement of 0.07 Å within 300 fs. A similar situation is found for one monolayer Fe on three layers of tungsten. The net spin percentage change due to the intraband (transport) contribution is only 0.1%. We find that although the crystal-momentum dispersed velocities are large, the strong cancellation of the velocities at two opposite crystal momentum points results in a small net velocity. Based on our numerical results and prior experimental findings [29], we propose a new picture to identify the pure transport-induced demagnetization through the ballistic transport [29], where both majority and minority spins travel at their respective velocities. This picture allows us to explain two latest experimental results [19, 22], without invoking SSD. Our study reveals crucial insights into the effect of the transport on the laser-induced demagnetization.

The rest of the paper is arranged as follows. In section 2, we present our theoretical formalism with details on the intraband transition. We show our results in section 3, where we examine the Fermi velocity and the velocity change under the laser excitation, followed by the spin moment change with and without intraband transitions. Section 4 is devoted to the discussion. Finally, we conclude this paper in section 5.

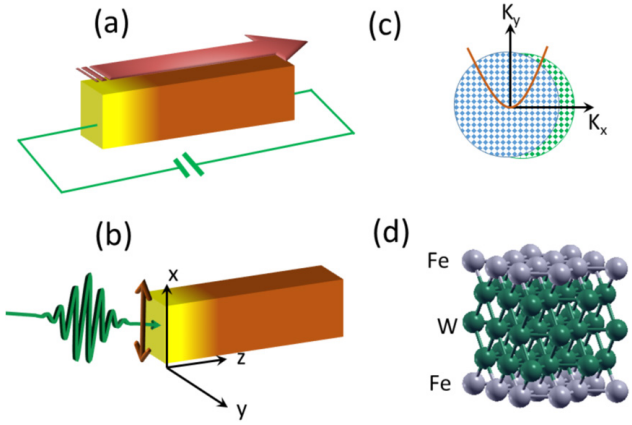

Figure 1. (a) Spin transport geometry under electric current. The bias is applied longitudinally, so electrons move in the opposite direction of the electric field. (b) Laser-induced spin transport. Here the laser electric field is perpendicular to the light propagation direction. The initial motion of the electron is vertical. (c) If the interband transition is ignored, the Fermi sphere shifts under an external field. However, in our simulation, we do not use this approach. (d) Supercell of one layer of Fe on three layers of W(1 1 0).

2. Theoretical formalism

In traditional spin transport, an external bias is applied longitudinally along a sample. Figure 1(a) illustrates such an example, where the electric field points to the left and the electrons move to the right. This is very different from laser-induced spin transport (see figure 1(b)). Light is a transverse wave, where its electric field (x axis) is perpendicular to the laser propagation direction (z axis). Therefore, initially electrons must move along the x axis, not along the z axis as assumed in several previous studies [14, 30, 31]. We note in passing that all the velocities here refer to the instantaneous velocities, not the time-averaged one. Only after this initial interaction with the laser field may the electrons that are close to the surface of a sample scatter with electrons that are away from the surface. It is this initial interaction of the electrons with the laser field that initiates laser-induced spin dynamics and spin transport, and underlies all the steps of laser-induced ultrafast demagnetization [1], a hot topic that remains unsolved up to now [32, 33].

Our theory starts with the standard density functional theory as implemented in the Wien2k code [34]. We first solve the Kohn–Sham equation (in atomic units) [35],

$$[-\nabla^2 + V_{ne} + V_{ee} + V_{xc}]\psi_{n\mathbf{k}}(r) = E_{n\mathbf{k}}\psi_{n\mathbf{k}}(r), \qquad (1)$$

to find the eigenvalues and eigenvectors. The terms on the left-hand side represent the kinetic energy, nuclear-electron attraction, electron–electron Coulomb repulsion and exchange correlation, respectively. We use the generalized gradient approximation (GGA) at the PBE level [36]. $\psi_{n\mathbf{k}}(r)$ represents the Bloch wavefunction of band n at crystal momentum $\mathbf{k}$, and $E_{n\mathbf{k}}$ is its band energy. These wavefunctions are used to construct the optical transition matrices for the time-dependent calculations. In the original Wien2k code, the matrix elements

($-\mathrm{i}\nabla$ operator) are stored with a precision to 10^{-6}. We modify the code so we can store the entire matrices unformatted, thus keeping all the 16 significant figures. The spin–orbit coupling (SOC) is included using a second-variational method, where spin-polarized eigenstates are used as the basis for the SOC calculation. The spin-matrix is constructed among band states by our home-built code that obeys the regular spin permutations [35].

To investigate the spin transport, we construct the electron velocity operator from the momentum operator as $\hat{v} = -\mathrm{i}\hbar\nabla/m_\mathrm{e}$, where m_e is the electron mass. In the absence of an external field, electrons on the Fermi surface travel with the Fermi velocity v_f, but their net velocity is zero because a nonzero velocity at a $\mathbf{k}$ point cancels another velocity at a $-\mathbf{k}$ point. There are several methods that we can use to compute the Fermi velocity. One is to take the derivative of the band energy $E_{n\mathbf{k}}$ with respect to $\mathbf{k}$. However, this may run into a singularity issue if the band dispersion is too steep, so we use a different method. After the convergence of our self-consistent calculation, we compute the momentum matrix elements between band states at each $\mathbf{k}$ point,

$$\langle n\mathbf{k}|\hat{\mathbf{P}}|m\mathbf{k}\rangle = \langle\psi_{n\mathbf{k}}| - \mathrm{i}\hbar\nabla|\psi_{m\mathbf{k}}\rangle, \tag{2}$$

where $\psi_{n\mathbf{k}}(r)$ and $\psi_{m\mathbf{k}}(r)$ are the wavefunctions for the band states $n\mathbf{k}$ and $m\mathbf{k}$, respectively. The diagonal matrix element of $\langle n\mathbf{k}|\hat{\mathbf{P}}|n\mathbf{k}\rangle$ is used to find the velocity $v_{n\mathbf{k}} = |\langle n\mathbf{k}|\hat{\mathbf{P}}|n\mathbf{k}\rangle/m_\mathrm{e}|$, where m_e is the electron mass. To compute the Fermi velocity, we integrate $v_{n\mathbf{k}}$ over $\mathbf{k}$ and sum over all those states on the Fermi surface,

$$v_\mathrm{f} = \sum_n \int \mathrm{d}\mathbf{k} v_{n\mathbf{k}} \delta(E_{n\mathbf{k}} - E_\mathrm{f}), \tag{3}$$

where E_f is the Fermi energy and $E_{n\mathbf{k}}$ is the band energy. The δ function is replaced by a broadening ϵ in the actual calculation, such that the states with energy $|(E_{nk} - E_\mathrm{f})| \leqslant \epsilon$ are included in the integration.

Our real time-dependent simulation starts with the Liouville equation for density matrices $\{\rho_\mathbf{k}\}$ at every $\mathbf{k}$ point [28, 35, 37, 38],

$$\mathrm{i}\hbar\frac{\partial\rho_\mathbf{k}}{\partial t} = [H_0 + H_I, \rho_\mathbf{k}] - \mathrm{i}e\mathbf{F}(t)\cdot\nabla_\mathbf{k}\rho_\mathbf{k} \tag{4}$$

where H_0 is the field-free system Hamiltonian. The interaction between the laser and system is $H_I = -e\mathbf{F}(t)\cdot\sum_\mathbf{k}\mathbf{D}_\mathbf{k}\rho_\mathbf{k}$, where $\mathbf{F}(t)$ is the laser electric field with the amplitude F_0 in V Å^{-1} and has a Gaussian shape with pulse duration τ in fs. The laser photon energy is $\hbar\omega$. The normal Liouville equation [35] is recovered if the second term on the right side of equation (4) is absent. This second term is the intraband transition term between different $\mathbf{k}$ points and is directly responsible for electron transport between different $\mathbf{k}$ points. However, this introduces a numerical complication that the density matrices at different $\mathbf{k}$ points are no longer separable, and numerical calculations become very time consuming since the $\mathbf{k}$ parallelization is not possible. A technical detail should be mentioned here [37, 38]. In equation (4), the second term on the right side should be treated with great care [38]. We use the fourth-order derivative solver and use a dense $\mathbf{k}$ mesh grid, which guarantees the accuracy of our calculation. In the case that interband transitions are ignored, the effect of the laser field is equivalent to shifting the Fermi sphere as shown in figure 1 (for details, see the appendix). In our calculation, we directly use equation (4), so both intraband and interband transitions are included. Our method is similar to the time-dependent density functional theory [39–42], and rigorously obeys the Pauli exclusion principle, so we can investigate the electron population change dynamically. We use the length gauge since it allows us to separate the intraband and interband transitions easily because they appear in two separate terms in our Liouville equation. For this reason, the length gauge has been frequently used for solids [37, 38, 43].

3. Results

Before a laser field interacts with a system, electrons on the Fermi surface travel with the Fermi velocity. The laser field exerts an additional force on those electrons. Most prior studies do not address some of the basic questions in transport. For instance, how fast do the itinerant electrons move under laser excitation? How far do they transport? In regular diffusion processes, there must be a gradient between different parts of a sample. Our goal is to develop a picture for electron transport on a solid ground and investigate how much the laser impacts the electron dynamics on the shortest time scale. We consider two systems, one bulk and one thin film. We choose bulk fcc Ni and a thin film with one monolayer of iron on top of three layers of tungsten in a slab geometry. We can not think of a better place to start with transport by looking at the Fermi velocity.

3.1. Fermi velocity in Ni

We start with fcc Ni. In our calculation, we adopt a simple cubic structure (4 Ni atoms per unit cell) to avoid the issue of the derivative of the density matrix with respect to the crystal momentum. We use the $\mathbf{k}$ points in the full Brillouin zone instead of the irreducible one for the same reason. The size of our problem is determined by the number of $\mathbf{k}$ points N_k and the number of bands N_b. The matrix size is $N_kN_b \times N_kN_b$. Given the limit of our computer resource, we can only adopt a $\mathbf{k}$ mesh of $16 \times 16 \times 16$ and $N_b = 60$. We remove 32 low-lying states (8 states, 2 for $3s$ and 6 for $3p$ per Ni atom), so these 60 states span across the Fermi level and reach all the way up to 1 Rydberg, which is more than enough to cover all the bands affected by the laser excitation.

In the discrete mesh, the Fermi surface is not clear cut. We have to use a broadening in the form of a shell around it. This broadening has a physical meaning as well if we consider it as a thermal broadening that can be changed. We use equation (3) to compute the Fermi velocity. Figure 2 shows our theoretical Fermi velocity in fcc Ni as a function of the broadening ϵ around the Fermi energy E_f. ϵ allows us to control the number of band states entering the integration in equation (3).

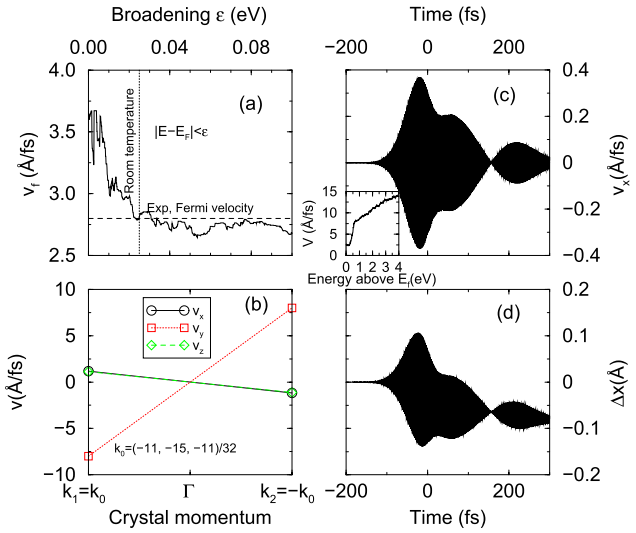

Figure 2. (a) Fermi velocity as a function of energy broadening ϵ in fcc nickel. The horizontal dashed line is the experimental Fermi velocity. (b) Electron velocity comparison between two $\mathbf{k}$ points in opposite directions. $\mathbf{k}_1 = (11, 15, 11)/32$ and $\mathbf{k}_2 = (-11, -15, -11)/32$ in the unit of the reciprocal lattice vector $b = 2\pi/a$, where a is the lattice constant of fcc Ni. These two $\mathbf{k}$ points have the largest velocity with band 70, which is at the Fermi level. (c) Collective velocity along the x axis upon laser excitation in fcc nickel. Inset: Velocity as a function of energy. Here the energy is referenced to the Fermi energy. (d) Collective displacement along the x axis. This is calculated by integrating the velocity over time.

We see that the Fermi velocity has a nontrivial dependence on ϵ, but in general it decreases with ϵ. The vertical dashed line denotes the room temperature broadening. The crossing point on the curve gives us our theoretical velocity $v_f = 2.79$ Å fs^{-1}, which is in an excellent agreement with the experimental value of 2.8 Å fs^{-1} by Petrovykh *et al* [44] (the horizontal dotted line in figure 2(a)). This demonstrates the high accuracy of our calculation.

Although the electrons around the Fermi surface move with v_f, there is no net current or transport. This is because for every velocity at $\mathbf{k}$ point, there is a velocity in the opposite direction $-\mathbf{k}$ point. Physically, electrons at $\pm\mathbf{k}$ move in opposite directions, so the net current is balanced out. Figure 2(b) shows one example of velocities for the energy band $n = 70$ at $\mathbf{k}_1 = [(11, 15, 11)/32]b$ and $\mathbf{k}_2 = [(-11, -15, -11)/32]b$, where b is the reciprocal lattice vector. We see indeed

$$\mathbf{v}(\mathbf{k}_1) = -\mathbf{v}(\mathbf{k}_2). \tag{5}$$

All three components are numerically exactly the same. Therefore, when one discusses how fast electrons move, one must consider electrons at both $\mathbf{k}$ and $-\mathbf{k}$ points. The net spin change carried by those two electrons must be summed up to zero in the absence of an external field. The actual velocity that one should use for spin transport is not v_f, but the net velocity is $v_{net} = v_{laser} - v_{withoutlaser}$. This is because $v_{withoutlaser}$ allows electrons to reach the thermal equilibrium, while the extra velocity due to the laser field allows electrons to move out of equilibrium. In the next subsection, we compute how fast the electrons move collectively.

3.2. Velocity change under laser field excitation

Central to transport is the electron motion. It is interesting to note that there has been no study based on SSD to directly compute the electron velocity. We fill this important gap. We choose a linearly x-polarized pulse of $\tau = 60$ fs, $F_0 = 0.03$ V Å^{-1} and $\hbar\omega = 2$ eV, propagating along the z axis. Our laser field amplitude is comparable to experimental values [3], and at the field maximum, this corresponds to the crystal momentum shift $\Delta k = 0.015$ Å^{-1}. Since the reciprocal lattice vector length in fcc Ni is $b = 2\pi/a = 2\pi/3.518\,82 = 1.7856$ Å^{-1}, Δk represents only 8.4/1000 of the Brillouin zone, extremely small. Light is a transverse wave, and its electric field must be perpendicular to the propagation direction. If the light propagates along the z axis, electrons experience no external force along the z axis initially. This observation has apparently evaded prior investigations [9, 13, 14, 29].

Our numerical result confirms the above observation. Figure 2(c) shows the system averaged velocity along the x axis, $v_x = \sum_k \mathrm{Tr}(\hat{v}^x_{\mathbf{k}}\rho_{\mathbf{k}})$, as a function of time. Velocities along the other directions are much smaller. Our laser pulse peaks at 0 fs. From the figure, we see that v_x increases sharply, already starting at -100 fs, and peaks at -20 fs, ahead of the laser peak. v_x oscillates rapidly between -0.4 Å fs^{-1} and 0.4 Å fs^{-1}. This velocity is only 14% the Fermi velocity.

The key premise of SSD is that laser-excited electrons in *sp* bands are transported and *d* electrons are treated as local [8]. The theory is based on a prior static calculation [45] where the *sp* electrons have a speed of 10 Å fs^{-1}. The argument is that if one puts electrons in states 2 eV (photon energy) above the Fermi level, they acquire this velocity. To be sure, we also calculate the same static crystal-momentum averaged velocity as a function of the energy referenced to the Fermi energy. The inset in figure 2(c) shows that electrons at 2 eV can indeed gain 10 Å fs^{-1}, consistent with Zhukov's finding [45], but whether all those *d* electrons can be excited to the sp bands at 2 eV has been unknown dynamically.

Our calculation gives an answer to this question. We find a much lower velocity, where the reason is very simple. In the laser excitation, there are lots more intermediate states occupied below 2 eV, and electrons in those states have a lower velocity. The static estimation overestimates the level of excitation. Even if the *sp* electrons move with such a high velocity, their contribution to spin change would be limited because *sp* electrons are not strongly spin polarized and have a very small effect on the demagnetization. This 10 Å fs^{-1} is 3.5 times larger than the Fermi velocity and 25 times larger than our calculated peak velocity. Furthermore, the velocity only peaks within a narrow time window, after which it subsides quickly. For our current laser parameter, this window is about 50 fs.

The velocity is not the only one that we can examine. To see whether electrons indeed diffuse away from their original location, we integrate the velocity v_x to get the collective displacement of the electrons,

$$\Delta x(t) = \int_{-\infty}^{t} v_x(t')\mathrm{d}t', \tag{6}$$

where $v_x(t')$ is the velocity along the x axis at time t'. Note that even though the velocity appears to be symmetric, if we zoom in, we find that there is an asymmetry in the velocity. This velocity drift accumulates as time evolves and leads to the net displacement. Figure 2(d) shows the displacement as a function of time. It is clear that the rapid oscillations of the electrons do not lead to a large net displacement in the position space. At the end of the pulse, the net displacement is less than 0.1 Å. In our simulation, we use a simple cubic structure (a supercell with four Ni atoms) to simulate a fcc structure, so we can investigate whether electrons transport from one lattice site to another. Ni's lattice constant is 3.52 Å, so the net transport effect is very small, which is consistent with our expectation. However, this does not mean that the electron transport does not occur, but it means that the laser-induced one is very small at the earliest stage. This is the time scale that SSD claims to be able to completely explain the demagnetization [8]. An additional challenge for SSD is the direction of the forces that electrons experience. Without laser excitation, the net force on the electrons has to be zero. As briefly discussed above, if a laser pulse propagates along the z axis, the laser electric field must be in the xy plane. For a tetragonal structure (with the spin–orbit coupling and magnetic quantization axes along the z axis, a fcc structure becomes tetragonal), the net force along the z axis is zero by the space symmetry, at least in the beginning of laser excitation. This questions the rationale that SSD always assumes the electron propagation direction to be along the light propagation direction.

3.3. Effect of electron transport on demagnetization in bulk nickel

So far, we have only investigated the electron dynamics, in particular, how the electron changes its velocity upon laser excitation. Next, we see how electron transport affects spin dynamics. We start from fcc Ni. The results are shown in figure 3. The solid line is the spin moment with the intraband term in equation (4), while the dashed line is without the intraband term. Figure 3(a) shows that both cases have a similar spin change, and their difference is very small mainly after the minimum. The recovered spin moment for the non-intraband transition is larger, i.e. smaller demagnetization. To see the detailed change, in figure 3(b) we plot their difference $\Delta M_z = M_z^{\text{intra}} - M_z^{\text{no intra}}$ as a function of time. The direct impact of transport is small, only about 3%. It is clear that the intraband contribution is mainly on a time scale longer than 100 fs, after the demagnetization maximum.

We further examine how the velocity disperses with the crystal momentum under the laser excitation. This information is crucial since it provides the details of electron dynamics. There are many crystal momentum directions that we can examine. We choose the Γ-X direction, since along this direction the laser field is applied. Figure 3(c) shows the first half of the Γ-X line, with the crystal momenta value given in the caption and denoted in the figure by k_i. Note that our k mesh is shifted for convergence purposes. k_1 approximately corresponds to the Γ point. We see that as we move away from the Γ point, the magnitude of the equilibrium velocities (the

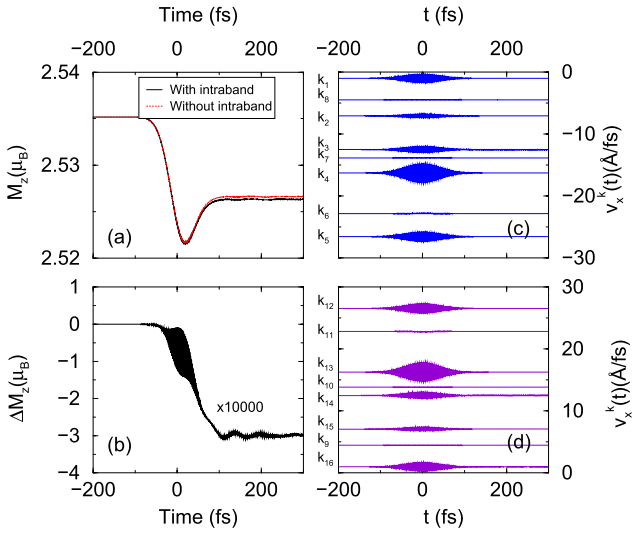

Figure 3. (a) Demagnetization with and without intraband transitions in fcc Ni. Our laser field is applied along the x axis. The field amplitude is 0.03 V Å^{-1} and duration is 60 fs. Solid line: with intraband contribution. Dotted line: without intraband transitions. Including intraband transitions increases the amount of demagnetization. Note that we use a simple cubic to simulate fcc Ni, where there are four atoms in the unit cell and the spin moment is four times larger than the fcc cell. (b) Difference between two spin moments, where the curve is multiplied by 10 000. The difference is very small. (c) Crystal-momentum-dispersed velocities as a function of time on the first half of the Γ-X line. $k_i = (i,1,1)b/32$, where i runs from 1 to 15 in steps of 2. b is the reciprocal lattice constant. (d) Crystal-momentum-dispersed velocities as a function of time on the second half of the Γ-X line. $k_i = (i,1,1)b/32$, where i runs from 17 to 31 in steps of 2.

base lines) is higher as expected. But it only increases up to k_5, after which the velocity starts to decrease, since the band starts to change. It is clear that at each **k** point, the electron velocity gain differs. We see that at k_6, k_7, and k_8, there is little gain, but the gain is large at k_4. This is directly connected to the band structure itself. So far, all the velocities are negative. If we examine the second half of the Γ-X line, we see that those velocities are all positive (see figure 3(d)). This is because the band dispersion changes its slope [35]. Now if we compare figures 3(c) and (d), these velocities are nearly opposite to each other. In other words, in a bulk material, the electrons move in the opposite directions. To have a net flow of electrons, the system must have an asymmetry.

3.4. Effect of electron transport on demagnetization in an Fe/W(1 1 0) ultrathin film

In the following, we investigate an ultrathin film, where we place a monolayer of Fe on the top of three layers of W(1 1 0) (see figure 1(d)). To maintain the inversion symmetry, it is customary that another layer of Fe is placed at the bottom of W. We adopt a supercell structure where we have added a vacuum layer to separate these slabs. The thickness of the vacuum layer is 11.19 Å, or five layers. We first optimize the structure along the z direction, assuming pseudomorphic growth. The optimized structure has the Fe atom shifted about 1% toward the W atom. The spin moment is mainly on the Fe

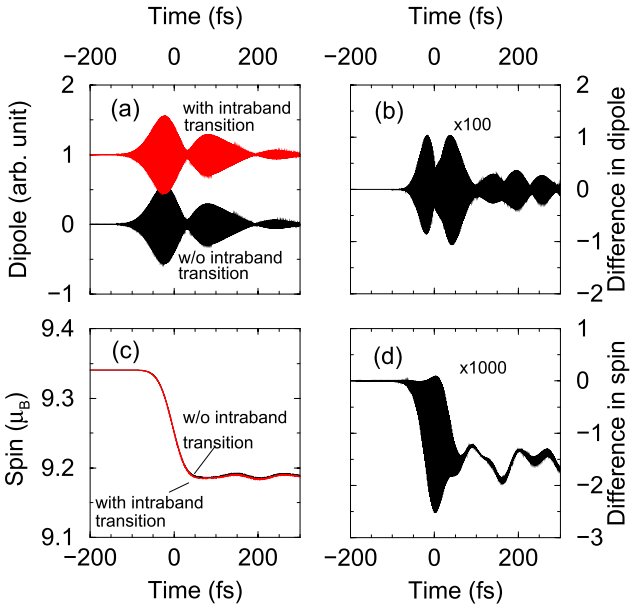

Figure 4. (a) Comparison between the dipole moments with and without intraband transitions in Fe/W(1 1 0). (b) Difference between the dipole moments, multiplied by 100. (c) Ultrafast demagnetization with and without intraband transitions. (d) Spin-moment difference.

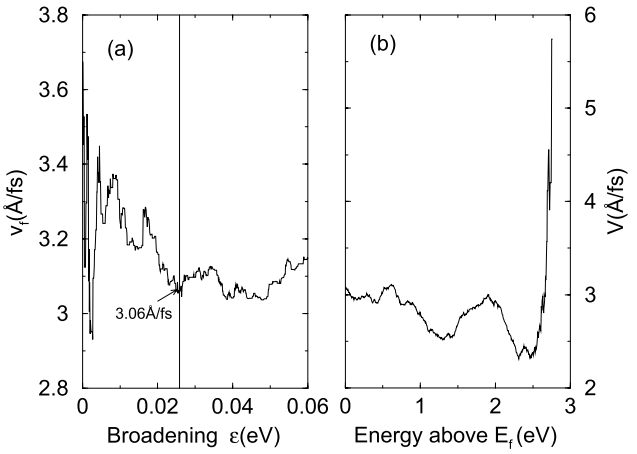

Figure 5. (a) Fermi velocity as a function of the broadening ϵ in the Fe/W(1 1 0) thin film. The vertical line denotes the room temperature, where we find the Fermi velocity is 3.06 Å fs^{-1}. This is higher than that in Ni. (b) Velocity as a function of the energy with respect to the Fermi energy. We include an energy window of 0.2 eV. We only plot the energy up to 3 eV.

atom, 2.5 μ_B, while the tungsten atom has a very small value of -0.1 μ_B. From the above study, we already see the small change in Ni due to the intraband transition, so we wonder whether there is any difference in the dipole moment (which reflects the optical response). Figure 4(a) compares two dipole moments, with and without the intraband transition. We shift the one with the intraband transition vertically by one unit for clarity. We see that there is no visual difference. Figure 4(b) shows their numerical difference, where we multiply the curve by a factor of 100. We see that the impact of intraband transitions on the dipole moment is more pronounced. The difference starts earlier before the laser pulse peaks. This is expected since the dipole reflects charge response as it responds faster than the spin [46].

The spin moment is plotted as a function of time in figure 4(c). The solid line (black) is the one without intraband transitions, while the dotted line (red) is the one with intraband transitions. We see that they almost overlap with each other. To see their difference, we multiply it by 1000 and show it in figure 4(d). We find the same conclusion is true for an Fe/W(1 1 0) thin film. The spin change due to the intraband transition is very small. However, we see the overall demagnetization is larger in the Fe/W(1 1 0) ultrathin film than that in Ni (compare figures 3(a) and 4(c)). We wonder whether this is connected with the Fermi velocity. Figure 5(a) is the Fermi velocity as a function of the broadening ϵ. The Fermi velocity at room temperature is highlighted with a vertical line. It is 3.06 Å fs^{-1}, which is indeed higher than that in Ni. Next, we also compute the velocity as a function of energy with respect to the Fermi energy. If the electrons are all excited to a particular energy, they will acquire this velocity. Figure 5(b) shows that at 2 eV, the velocity is less than 3 Å fs^{-1}, less than that at the same energy in Ni. This demonstrates that if the velocity at the high energy window is crucial to the demagnetization, then we should expect a larger demagnetization in Ni. Our data do not support such a scenario.

4. Discussions: necessity of ultrashort pulses

In retrospect, many earlier claims have been overstated, without leaving sufficient room for new ideas. When we examine the SSD theory closely, we notice in the initial step how the *sp* electrons are excited by a laser pulse is missing. Instead, the entire generation process is controlled by a source term $S^{\rm ext}$ which is not given in their publications [8, 9]. This prevents one from examining their theory further. However, it becomes clear now that they made an important assumption that each Ni atom takes 0.1 photon (with photon energy of 1.5 eV) and each Fe atom takes 1 photon in their theory [9]. As we showed recently, this 0.1 photon is sufficient to reproduce all the demagnetization process in Fe, Co and Ni [28], even without invoking spin superdiffusion. In the Hübner model [2], the laser excitation enters through the dipole interaction term. The conservation of angular momentum is achieved through the dipole transitions, where the laser field and the magnetic system exchange orbital angular momentum. The linear momentum of the photons at our wavelength is extremely small, in comparison with the electron momentum, and is ignored here. A similar approach was employed in the time-dependent density functional theory calculation [22]. This is the standard method that one can systematically increase the laser amplitude as we did before [47]. Both the theory [47] and experiment [48] showed that a shorter laser pulse induces a much steeper demagnetization, which is significantly different from those with a longer laser pulse where a more gradual decrease in magnetization is observed. A similar laser-fluence dependence in SSD is unknown.

To understand the role of transport in the demagnetization, we face multiple challenges. First, both the spin–orbit coupling induced demagnetization [2] and the spin

superdiffusion-induced demagnetization [8] occur on a similar time scale, so it is difficult to separate them in the time domain. Second, there is a difference between (a) using hot electron transport to demagnetize a sample and (b) proving that the demagnetization exclusively comes from hot electron transport. (a) is similar to transient electron doping. Nickel and copper differ by one valence electron, but one is magnetic and the other is not. There is no surprise here. (b) is more tricky since there are many possible ways that a magnet can be demagnetized. To demonstrate that demagnetization comes from electron transport requires an exhaustive effort to exclude all the possible channels. Vodungbo *et al* [49] stated clearly that even though indirect excitation can lead to ultrafast demagnetization, this can not be used as evidence for SSD, since the amount of gain and loss in spin polarization must both be measured to quantitatively determine the relevance/contribution of superdiffusive spin transport to the overall demagnetization. Since demagnetization and spin transport occur on a similar time scale, it is necessary to employ a shorter pulse to disentangle their difference.

Next, we outline what should happen if the demagnetization is due to the ballistic transport alone, given that most of samples are very thin. Figure 6(a) shows a case for the ballistic transport with a short magnetic sample with length l_{m}. We assume that the laser pumps on the front (the left side) and the detection can be either in the front or the back. The times for the majority and minority spins to travel through the sample are

$$t_{\uparrow} = l_{\mathrm{m}}/v_{\uparrow} \quad \text{and} \quad t_{\downarrow} = l_{\mathrm{m}}/v_{\downarrow}, \tag{7}$$

respectively. We take the experimental parameters from Shokeen *et al* [22]. The thickness of their film is 10 nm. By using the velocities for the majority and minority spins [45], the time delay Δt_{sp} of the minority *sp* spin at 1.5 eV with respect to the majority *sp* spin is 2.6 fs. Therefore, from 0 to 10.5 fs ($t_{\uparrow}(sp)$), the back side of the sample should show the spin moment enhancement. After 2.6 fs, the minority spins arrive and the enhancement stops, so the spin moment returns back to the pre-pump value. In the meantime, the front probe should see the demagnetization. If the pump is strong, the magnetic moment should drop to zero and reverse the sign, since the minority becomes the majority as the true majority spin moves out of the region. This 2.6 fs is way too short for many experiments to detect *sp* spin transport. However, if the transport is carried by the 3*d* electron spins, which is not included in the original SSD theory [8], then Δt_{3d} is 54.1 fs. This time delay is within the regime of the experiment [22]. The 42 fs spin enhancement peak observed in the gold layer by Hofherr *et al* [19], which is very close to our time of 54.1 fs, is now explainable, since incidentally their nickel thin film thickness is exactly the same as that of Shokeen *et al* [22]. It is more likely that both majority and minority spins reach the gold layer. We will come back to this below.

In figure 6(b), we schematically show the magnetization change as a function of time for the front probe and back probe. The ideal experimental detection is on the back side. The front side probe suffers from the charge depletion as majority and minority spins move out of the regime. If an insulator is attached to the front, this creates a capacitor effect that pulls both majority and minority spins back, so the magnetic moment crosses zero again. If a conductor is attached to the front, the electron flow from the conductor to the ferromagnetic sample further complicates the entire process. On the other hand, the back side probe is relatively cleaner because charge carriers tend to move out of the sample. It must show a hump at Δt if the demagnetization is dominated by the spin transport. From the experimental data [22], if the *sp* spin transport is important, the peak location is beyond the current laser pulse duration; if the 3*d* spin transport is important, this should be detectable, but this was not observed experimentally in Ni [18, 22].

For Co, we do not have a good experimental velocity. Sant *et al* [50] estimated the spin diffusion coefficients at 500 fs, far beyond the superdiffusion limit. Although they implied the results are from the domain wall, it is more likely that they detected the spatial spin distribution, rather than the domain wall motion, since the domain wall can not move so fast. They estimated the spin diffusion coefficient D (at 500 fs) to be 0.35 $\mathrm{nm}^2\ \mathrm{fs}^{-1}$ for spin up and 0.02 $\mathrm{nm}^2\ \mathrm{fs}^{-1}$. We can compute the spin velocity through

$$v_{\uparrow(\downarrow)} = \sqrt{D_{\uparrow(\downarrow)}/t(500\ \mathrm{fs})}, \tag{8}$$

which gives $v_{\uparrow} = 0.26$ Å fs^{-1} and $v_{\downarrow} = 0.063$ Å fs^{-1}. These velocities are in line with our theoretical findings (see figure 2(c)), though we have a different system and their velocities already pass their maxima. For the same thickness of 10 nm, if the majority and minority spins moved with these velocities to traverse the entire sample, the time delay Δt between the spin up and spin down would be 1209 fs. Next, we extrapolate their diffusion coefficient all the way to 0 ps by a quadratic function, and applying the same equation (equation (8)), we find the time delay is reduced to 753.9 fs. This surely over-estimates the delay, but it does point out that the delay in Co is qualitatively longer than that in Ni. If we use the theoretical estimate for the majority spin $v_{\uparrow} = 2.55$ Å fs^{-1} [51], we can figure out the velocity for the minority spin. Shokeen *et al* [22] found there is a small enhancement within 20 fs experimentally, so the $v_{\downarrow} = 1.69$ Å fs^{-1}, which is well within our expectation if we compare it with 1.44 Å fs^{-1} of Ni. In other words, the pure ballistic spin transport contribution should be over within 20 fs. This time scale is still too short for many prior experiments [12–14].

Now with the spin enhancement time understood, we can address the spin moment loss. Hofherr *et al* [19] found that the spin moment loss in Ni is 0.52 μ_{B}/atom, but the spin increase in the Au film is 0.015 μ_{B}/atom, only 2.8%, with the 97.2% spin loss unaccounted for. Given that MOKE is bulk-sensitive, such a huge discrepancy is surprising. One possible explanation from our picture is that the main spin loss in Ni is in the 3*d* states and is local. A small portion of frontier 3*d* electrons, including both majority and minority spins, enters the Au layer. The spin enhancement peak is formed due to the arrival of minority spins; once the majority spin leaves, the minority spin dominates and leads to the spin reversal. For this reason, the density of states across the Fermi level

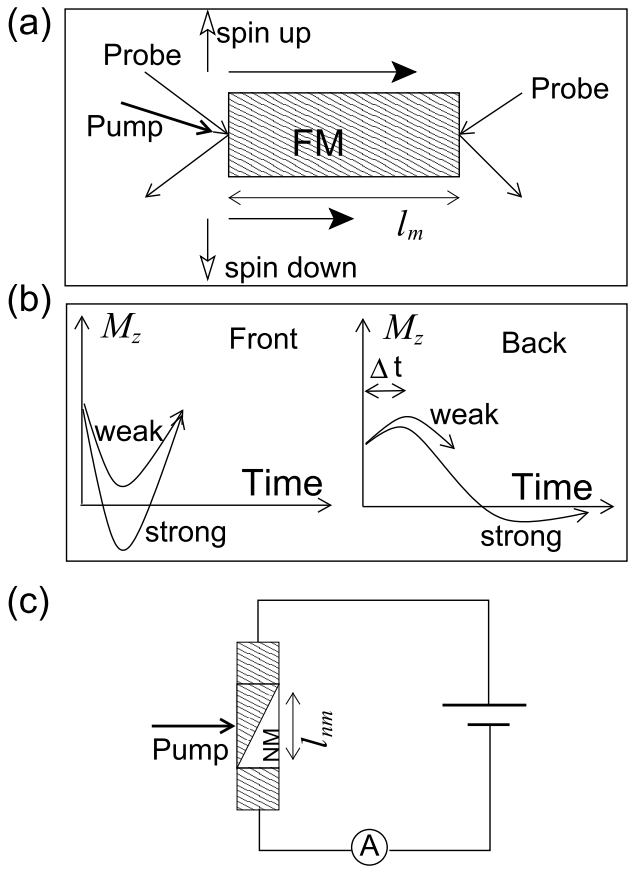

Figure 6. Theoretical proposal for testing if only the pure spin transport contributes to the ultrafast demagnetization. (a) Geometry of the proposed experiment. Similar to the experimental detection scheme, the pump is always on the front. The detection can be either on the front or on the back. Majority and minority spins move at different velocities. (b) Predicted effect of transport on demagnetization. For the front probe, the spin drops and returns to its original value after the minority spin departs. For the back probe, one should see an enhancement within the delay between the majority and minority spins. (c) Proposed experiment to detect the spin injection into the nonmagnetic layers as a function of the thickness of both magnetic and nonmagnetic layers. The pump can be on the side of the nonmagnetic layer as well.

is crucial to the spin transport as shown recently for Gd [52] and in Co/Cu(0 0 1) interfaces [23]. More definitive answers require a detailed calculation of density of states at the interface between the Ni and Au layers.

Finally, to quantify the amount of the spin transported into a nonmagnetic layer, we propose a spin-valve structure. Figure 6(c) shows such a structure. A ferromagnetic layer is grown on the wedged nonmagnetic layer of length $l_{\rm nm}$, and is pumped by a laser pulse. One can also pump on the nonmagnetic layer. Depending on the location that the laser beam aims at, one can systematically control the amount of the spin current flowing into the nonmagnetic layer by measuring the magneto-resistance in the circuit. However, this experiment may not be easy since the electric current detection is normally much slower than the optical stimulus, but at least this gives some quantitative measure of how much the spin propagates into the nonmagnetic layer.

5. Conclusions

We have carried out a first-principles calculation to investigate whether transport through the intraband transition affects the demagnetization. We employ two systems, one bulk and one ultrathin film. We find that in both systems the effect of transport on demagnetization is very small, less than 1%. The maximum velocity in Ni is 0.4 Å $\rm fs^{-1}$. This is much smaller than that assumed in the SSD theory, where all the *sp* electrons gain 10 Å $\rm fs^{-1}$. In addition, the velocity oscillates strongly, so the net displacement for the electron is very small. We should point out that it is the net velocity gained by the electron that is related to the transport, not the Fermi velocity, since in the crystal momentum space the velocities should be symmetric without an external field. The charge response is more pronounced and also faster than the spin. Following the latest experimental findings [22], we suggest the entire demagnetization should be separated into two categories, photo-doping and photo-excitation. In photo-excitation, the electrons are excited to excited states and then the demagnetization starts, while in photo-doping, the electrons transport from one material to another, so this process depends critically on the materials in question. For instance, whether the Fe layer or Ni layer is excited first matters to the entire demagnetization process, since they have different Fermi energies. We trust that our finding will motivate further experimental and theoretical investigations.

Acknowledgments

We appreciate the helpful communications with Dr T T Luu and Dr M Dignam on the intraband transition [37, 38]. This work was solely supported by the U.S. Department of Energy under Contract No. DE-FG02-06ER46304. Part of the work was done on Indiana State University's high performance quantum and obsidian clusters. The research used resources of the National Energy Research Scientific Computing Center, which is supported by the Office of Science of the U.S. Department of Energy under Contract No. DE-AC02-05CH11231.

Appendix. Pure intraband transitions

If we do not have the first term on the right side of equation (4) and only keep the diagonal terms of $\rho_{\mathbf{k}}$, then we recover the classical Boltzmann equation. Here the time evolution is determined by

$$\hbar\frac{\partial\rho_{\mathbf{k}}}{\partial t} + e\mathbf{F}(t)\cdot\nabla_{\mathbf{k}}\rho_{\mathbf{k}} = 0, \tag{A.1}$$

which is the standard first-order homogeneous equation [53],

$$\frac{\partial u}{\partial x} + p(x,y)\frac{\partial u}{\partial y} = 0, \tag{A.2}$$

where in general the unknown u and known p are both functions of x and y. Mathematically, equations like this have an

exact solution, which is found by the method of characteristic curves. The key idea is that one finds a path or curve (defined by (x, y)) where $u(x, y)$ is constant. On this curve, how y changes depends on how x changes. Their relation is determined by the derivative of y with respect to x, $\mathrm{d}y/\mathrm{d}x = p(x, y)$.

Here is a brief explanation. First, let us consider a simple case where $p(x, y) = 1$, so we have [53]

$$\frac{\partial u}{\partial x} + \frac{\partial u}{\partial y} = 0, \tag{A.3}$$

where $u = u(x, y)$ is the unknown function. According to Asamar [53], if f is any differentiable function of a single variable, then

$$u(x, y) = f(x - y) \tag{A.4}$$

is a solution of equation (A.3). We can verify this by using the chain rule, where we get that

$$\frac{\partial u}{\partial x} = f'(x - y); \frac{\partial u}{\partial y} = -f'(x - y). \tag{A.5}$$

We see that equation (A.3) holds with this solution. Note that the functions are constant on any line $(x - y = c)$ due to the form of the solution $u(x, y) = f(x - y)$. Here c is constant. The actual form of $u(x, y)$ is determined by the initial condition. One example in physics is the Fermi function $f(E) = \frac{1}{1+\exp(E-E_\mathrm{f})}$, where E is the band energy and E_f is the Fermi energy.

If $p(x, y) = 2$, then the variable in equations (A.4) and (A.5) is $(2x - y)$. In other words, on the characteristic line x must move two units for every one unit along the y direction. For all the other cases, one can derive a similar relation.

Next, we consider a generic case with nonconstant $p(x, y)$. Here the above line becomes a curve where x and y change according to the constraint $\mathrm{d}y/\mathrm{d}x = p(x, y)$. In other words, the rate of change of y with respect to x is just $\mathrm{d}y/\mathrm{d}x = p(x, y)$. On the curves (x, y) with the constraint $\mathrm{d}y/\mathrm{d}x = p(x, y)$, u is constant. If we suppose the solution of $\mathrm{d}y/\mathrm{d}x = p(x, y)$ is $\phi(x, y)$, as far as $\phi(x, y)$ is constant on the characteristic curve, we have a solution $u(x, y) = f(\phi(x, y))$, where the functional of f can be an arbitrary function. As discussed above, the actual form is fixed by the initial condition, in our case, a Fermi function, so $\rho_\mathbf{k}$ does not change its shape, regardless of what the external field looks like. When we apply $\mathrm{d}y/\mathrm{d}x = p(x, y)$ to our problem, p is $e\mathbf{F}(t)/\hbar$, so we get

$$\frac{\partial \mathbf{k}}{\partial t} = \frac{e\mathbf{F}(t)}{\hbar} = -\frac{e}{\hbar}\frac{\mathbf{A}(t)}{\partial t}, \tag{A.6}$$

which, after integration, leads to our familiar form of

$$\mathbf{k} + e\mathbf{A}(t)/\hbar = \mathbf{k}_0. \tag{A.7}$$

$\mathbf{A}(t)$ in equation (A.6) is the vector potential of the laser field $\mathbf{F}(t)$. If we relabel the original $\mathbf{k}$ in $\rho_\mathbf{k}$ by $\mathbf{k}_0$, our solution is $\rho_\mathbf{k} = \rho_\mathbf{k}(f(\mathbf{k} + e\mathbf{A}(t)/\hbar))$. Here, in absence of interband transitions, $\rho_\mathbf{k}$ is always a Fermi distribution function. This solution is exact mathematically, independent of the form of $\mathbf{A}(t)$, constant or oscillatory. Physically, in the absence of interband transitions, such transitions are equivalent to shifting the electron Fermi surface in the reciprocal space along the external field direction. Figure 1(c) illustrates such a situation. The amount of shift is determined by the laser vector potential. With the presence of the interband transitions, such shifting no longer works, so one has to use equation (4), which is exactly what we do here.

ORCID iDs

G P Zhang https://orcid.org/0000-0003-2864-9605

References

[1] Beaurepaire E, Merle J C, Daunois A and Bigot J-Y 1996 Ultrafast spin dynamics in ferromagnetic nickel *Phys. Rev. Lett.* **76** 4250
[2] Zhang G P and Hübner W 2000 Laser-induced ultrafast demagnetization in ferromagnetic metal *Phys. Rev. Lett.* **85** 3025
[3] Koopmans B, Malinowski G, Dalla Longa F, Steiauf D, Fähnle M, Roth T, Cinchetti M and Aeschlimann M 2010 Explaining the paradoxical diversity of ultrafast laser-induced demagnetization *Nat. Mater.* **9** 259
[4] Essert S and Schneider H C 2011 Electron–phonon scattering dynamics in ferromagnetic metals and their influence on ultrafast demagnetization processes *Phys. Rev.* B **84** 224405
[5] Baral A, Vollmar S and Schneider H C 2014 Magnetization dynamics and damping due to electron–phonon scattering in a ferrimagnetic exchange model *Phys. Rev.* B **90** 014427
[6] Si M S and Zhang G P 2010 Resolving photon-shortage mystery in femtosecond magnetism *J. Phys.: Condens. Matter* **22** 076005
[7] Zhang G P and George T F 2008 Total angular momentum conservation in laser-induced femtosecond magnetism *Phys. Rev.* B **78** 052407
[8] Battiato M, Carva K and Oppeneer P M 2010 Superdiffusive spin transport as a mechanism of ultrafast demagnetization *Phys. Rev. Lett.* **105** 027203
[9] Battiato M, Carva K and Oppeneer P M 2012 Theory of laser-induced ultrafast superdiffusive spin transport in layered heterostructures *Phys. Rev.* B **86** 024404
[10] Melnikov A, Razdolski I, Wehling T O, Papaioannou E T, Roddatis V, Fumagalli P, Aktsipetrov O, Lichtenstein A I and Bovensiepen U 2011 Ultrafast transport of laser-excited spin-polarized carriers in Au/Fe/MgO(0 0 1) *Phys. Rev. Lett.* **107** 076601
[11] Vodungbo B *et al* 2012 Laser-induced ultrafast demagnetization in the presence of a nanoscale magnetic domain network *Nat. Commun.* **3** 999
[12] Pfau B *et al* 2012 Ultrafast optical demagnetization manipulates nanoscale spin structure in domain walls *Nat. Commun.* **3** 1100
[13] Rudolf D *et al* 2012 Ultrafast magnetization enhancement in metallic multilayers driven by superdiffusive spin current *Nat. Commun.* **3** 1037
[14] Eschenlohr A, Battiato M, Maldonado P, Pontius N, Kachel T, Holldack K, Mitzner R, Föhlisch A, Oppeneer P M and Stamm C 2013 Ultrafast spin transport as key to femtosecond demagnetization *Nat. Mater.* **12** 332
[15] Zhang G P, Hübner W, Lefkidis G, Bai Y and George T F 2009 Paradigm of the time-resolved magneto-optical Kerr effect for femtosecond magnetism *Nat. Phys.* **5** 499
[16] Bigot J-Y, Vomir M and Beaurepaire E 2009 Coherent ultrafast magnetism induced by femtosecond laser pulses *Nat. Phys.* **5** 515

[17] Turgut E *et al* 2013 Controlling the competition between optically induced ultrafast spin-flip scattering and spin transport in magnetic multilayers *Phys. Rev. Lett.* **110** 197201

[18] Schellekens A J, Verhoeven W, Vader T N and Koopmans B 2013 Investigating the contribution of superdiffusive transport to ultrafast demagnetization of ferromagnetic thin films *Appl. Phys. Lett.* **102** 252408

[19] Hofherr M *et al* 2017 Speed and efficiency of femtosecond spin current injection into a nonmagnetic material *Phys. Rev.* B **96** 100403

[20] Moisan N, Malinowski G, Mauchain J, Hehn M, Vodungbo B, Lüning J, Mangin S, Fullerton E E and Thiaville A 2014 Investigating the role of superdiffusive currents in laser induced demagnetization of ferromagnets with nanoscale magnetic domains *Sci. Rep.* **4** 4658

[21] von Korff Schmising C *et al* 2014 Imaging ultrafast demagnetization dynamics after a spatially localized optical excitation *Phys. Rev. Lett.* **112** 217203

[22] Shokeen V, Sanchez Piaia M, Bigot J-Y, Müller T, Elliott P, Dewhurst J K, Sharma S and Gross E K U 2017 Spin flips versus spin transport in nonthermal electrons excited by ultrashort optical pulses in transition metals *Phys. Rev. Lett.* **119** 107203

[23] Chen J, Bovensiepen U, Eschenlohr A, Müller T, Elliott P, Gross E K U, Dewhurst J K and Sharma S 2018 Competing spin transfer and dissipation at Co/Cu(0 0 1) interfaces on femtosecond timescales (arXiv:1803.03090v2)

[24] Tengdin P *et al* 2018 Critical behavior within 20 fs drives the out-of-equilibrium laser-induced magnetic phase transition in nickel *Sci. Adv.* **4** eaap9744

[25] Zhang W, He W, Peng L-C, Zhang Y, Cai J-W, Evans R F L, Zhang X-Q and Cheng Z-H 2018 The indispensable role of the transversal spin fluctuations mechanism in laser-induced demagnetization of Co/Pt multilayers with nanoscale magnetic domains *Nanotechnology* **29** 275703

[26] Gang S-G *et al* 2018 Element-selective investigation of femtosecond spin dynamics in NiPd magnetic alloys using extreme ultraviolet radiation *Phys. Rev.* B **97** 064412

[27] Fert T, Bergeard N, Malinowski G, Abrudan R, Kachel T, Holldack K, Hehn M and Boeglin C 2017 Ultrafast hot-electron induced quenching of Tb 4 *f* magnetic order *Phys. Rev.* B **96** 144427

[28] Zhang G P, Bai Y H and George T F 2016 Ultrafast reduction of exchange splitting in ferromagnetic nickel *J. Phys.: Condens. Matter* **28** 236004

[29] Bergeard N, Hehn M, Mangin S, Lengaigne G, Montaigne F, Lalieu M L M, Koopmans B and Malinowski G 2016 Hot-electron-induced ultrafast demagnetization in Co/Pt multilayers *Phys. Rev. Lett.* **117** 147203

[30] Seifert T *et al* 2018 Terahertz spectroscopy for all-optical spintronic characterization of the spin-Hall-effect metals Pt, W and $Cu_{80}Ir_{20}$ (arXiv:1805.02193v1)

[31] Li G, Mikhaylovskiy R V, Grishunin K A, Costa J D, Rasing T and Kimel A V 2018 Laser induced THz emission from femtosecond photocurrents in Co/ZnO/Pt and Co/Cu/Pt multilayers (arXiv:1711.08342v3 [cond-mat.mes-hall])

[32] Zhang G P, Hübner W, Beaurepaire E and Bigot J-Y 2002 Laser-induced ultrafast demagnetization: femtomagnetism, a new frontier? *Top. Appl. Phys.* **83** 245

[33] Kirilyuk A, Kimel A V and Rasing T 2010 Ultrafast optical manipulation of magnetic order *Rev. Mod. Phys.* **82** 2731
Kirilyuk A, Kimel A V and Rasing T 2016 Ultrafast optical manipulation of magnetic order *Rev. Mod. Phys.* **88** 039904 (erratum)

[34] Blaha P, Schwarz K, Madsen G K H, Kvasnicka D and Luitz J 2001 *WIEN2k, an Augmented Plane Wave + Local Orbitals Program for Calculating Crystal Properties* ed K Schwarz (Austria: Techn. Universität Wien)

[35] Zhang G P, Bai Y H and George T F 2009 Energy- and crystal momentum-resolved study of laser-induced femtosecond magnetism *Phys. Rev.* B **80** 214415

[36] Perdew J P, Burke K and Ernzerhof M 1996 Generalized gradient approximation made simple *Phys. Rev. Lett.* **77** 3865

[37] Al-Naib I, Sipe J E and Dignam M M 2014 High harmonic generation in undoped graphene: interplay of inter- and intraband dynamics *Phys. Rev.* B **90** 245423

[38] Luu T T and Wörner J J 2016 High-order harmonic generation in solids: a unifying approach *Phys. Rev.* B **94** 115164

[39] Krieger K, Dewhurst J K, Elliott P, Sharma S and Gross E K U 2015 Laser-induced demagnetization at ultrashort time scales: predictions of TDDFT *J. Chem. Theory Comput.* **11** 4870

[40] Elliott P, Müller T, Dewhurst J K, Sharma S and Gross E K U 2016 Ultrafast laser-induced local magnetization dynamics in Heusler compounds *Sci. Rep.* **6** 38911

[41] Krieger K, Elliott P, Müller T, Singh N, Dewhurst J K, Gross E K U and Sharma S 2017 Ultrafast demagnetization in bulk versus thin films: an *ab initio* study *J. Phys.: Condens. Matter* **29** 224001

[42] Dewhurst J K, Elliott P, Shallcross S, Gross E K U and Sharma S 2018 Laser-induced intersite spin transfer *Nano Lett.* **18** 1842

[43] Golde D, Meier T and Koch S W 2008 High harmonics generated in semiconductor nanostructures by the coupled dynamics of optical inter- and intraband excitations *Phys. Rev.* B **77** 075330

[44] Petrovykh D Y, Altmann K N, Höchst H, Laubscher M, Maat S, Mankey G J and Himpsel F J 1998 Spin-dependnent band structure, Fermi surface and carrier lifetime of permalloy *Appl. Phys. Lett.* **73** 34559

[45] Zhukov V P, Chulkov E V and Echenique P M 2006 Lifetimes and inelastic mean free path of low-energy excited electrons in Fe, Ni, Pt, and Au: *ab initio* GW + T calculations *Phys. Rev.* B **73** 125105

[46] Hübner W and Zhang G P 1998 Femtosecond spin dynamics probed by linear and nonlinear magneto-optics *J. Magn. Magn. Mater.* **189** 101

[47] Zhang G P, Lefkidis G, Hübner W and Bai Y 2011 Ultrafast demagnetization in ferromagnets and magnetic switching in nanoclusters when the number of photons is kept fixed *J. Appl. Phys.* **109** 07D303

[48] Fognini A, Salvatella G, Gort R, Michlmayr T, Vaterlaus A and Acremann Y 2015 The influence of the excitation pulse length on ultrafast magnetization dynamics in nickel *Struct. Dyn.* **2** 024501

[49] Vodungbo B *et al* 2016 Indirect excitation of ultrafast demagnetization *Sci. Rep.* **6** 18970

[50] Sant T *et al* 2017 Measurements of ultrafast spin-profiles and spin-diffusion properties in the domain wall area at a metal/ferromagnetic film interface *Sci. Rep.* **7** 15064

[51] Gall D 2016 Electron mean free path in elemental metals *J. Appl. Phys.* **119** 085101

[52] Zhang G P, Jenkins T, Bennett M and Bai Y H 2017 Manifestation of intra-atomic 5d6s-4f exchange coupling in photoexcited gadolinium *J. Phys.: Condens. Matter* **29** 495807

[53] Asmar N H 2000 *Partial Differential Equations and Boundary Value Problems* (Upper Saddle River, NJ: Prentice-Hall)